Extraction of electromagnetic transition form factors for nucleon resonances within a dynamical coupled-channels model

N. Suzuki,[1,2] T. Sato,[1,2] and T.-S. H. Lee[2,3]

[1]*Department of Physics, Osaka University, Toyonaka, Osaka 560-0043, Japan*

[2]*Excited Baryon Analysis Center (EBAC), Thomas Jefferson National Accelerator Facility, Newport News, Virginia 23606, USA*

[3]*Physics Division, Argonne National Laboratory, Argonne, Illinois 60439, USA*

(Received 11 June 2010; revised manuscript received 4 September 2010; published 22 October 2010)

We explain the application of a recently developed analytic continuation method to extract the electromagnetic transition form factors for the nucleon resonances (N^*) within a dynamical coupled-channel model of meson-baryon reactions. Illustrative results of the obtained $N^* \to \gamma N$ transition form factors, defined at the resonance pole positions on the complex energy plane, for the well-isolated P_{33} and D_{13} and the complicated P_{11} resonances are presented. A formula was developed to give a unified representation of the effects due to the first two P_{11} poles, which are near the $\pi\Delta$ threshold, but are on different Riemann sheets. We also find that a simple formula, with its parameters determined in the Laurent expansions of the $\pi N \to \pi N$ and $\gamma N \to \pi N$ amplitudes, can reproduce to a very large extent the exact solutions of the considered model at energies near the real parts of the extracted resonance positions. We discuss the important differences between our approach, which is consistent with the earlier formulations of resonances, and the phenomenological approaches using the Breit-Wigner parametrization of resonant amplitudes to fit the data.

DOI: 10.1103/PhysRevC.82.045206 PACS number(s): 13.75.Gx, 13.60.Le, 14.20.Gk

I. INTRODUCTION

The spectrum and form factors of excited nucleons are fundamental quantities for investigating the hadron structure within quantum chromodynamics (QCD). The excited nucleons are unstable and couple strongly to meson-baryon continuum states to form nucleon resonances (called collectively as N^*) in πN and γN reactions. It is well known that resonances locate on the unphysical sheets of the complex energy plane and thus their properties can only be extracted from the empirical partial-wave amplitudes by analytic continuation. Recently we applied an analytic continuation method developed in Ref. [1] to extract N^* pole positions [2] from πN elastic scattering amplitudes determined in a fit [3] (JLMS) within a dynamical coupled-channel model [4] (Excited Baryon Analysis Center-dynamical coupled-channel, EBAC-DCC) of meson-baryon reactions.

The scattering amplitudes obtained from a DCC model of meson-baryon reactions, such as the EBAC-DCC model as well as the models developed in Refs. [5–9], are not available in an analytic form. They are obtained numerically by solving coupled-channels integral equations with meson-exchange driving terms. Thus, the predicted amplitudes can only be analytically continued to the complex energy plane numerically with a careful account of the analytic structure of the considered scattering equations. Obviously, the method depends on the dynamical content of each model. For the EBAC-DCC model, this was developed in Ref. [1] and established using several exactly soluble models. In this article, we explain how this method is used to extract the $\gamma^* N \to N^*$ transition form factors from the multipole amplitudes determined from extending the JLMS analysis to investigate $\gamma N \to \pi N$ [10] and $N(e, e'\pi)N$ [11] reactions.

The electromagnetic $\gamma^* N \to N^*$ transition form factors give information on the current and charge distributions of N^* and N. It can be shown [12,13] that a resonance state $|\psi^R_{N^*}\rangle$ with a complex energy M_R can be defined as an "eigenstate" of the Hamiltonian $H|\psi^R_{N^*}\rangle = M_R|\psi^R_{N^*}\rangle$ with the outgoing boundary condition for its asymptotic wave functions. Therefore the $\gamma^* N \to N^*$ transition form factor is defined by the current matrix element $\langle\psi^R_{N^*}|J_{\rm em}|N\rangle$, which can be extracted from the residue $R_{\pi N,\gamma^* N}$ of electromagnetic pion production amplitudes at the resonance poles. To extract $R_{\pi N,\gamma^* N}$, we need to evaluate the on-shell matrix elements of the $\gamma^* N \to \pi N$ amplitudes on the complex Riemann energy sheet. As will be discussed later, the analytic structure of the considered coupled-channels equations for getting these on-shell matrix elements is rather complex and must be dealt with carefully. In particular, we need to develop a formula to give a unified representation of the first two P_{11} resonances that are near the $\pi\Delta$ threshold, but are on different Riemann sheets.

To illustrate our approach it is sufficient to only present results for the well-isolated resonances in P_{33} and D_{13} and the complex P_{11} partial waves. With only three complex parameters determined in the Laurent expansion of each partial-wave amplitude at resonance pole position, we present a simple formula that can reproduce to a very large extent the exact solutions of the considered model at energies near the real parts of the extracted resonance positions. This finding agrees with what was reported in an analysis [14] of the πN scattering amplitude within the Jülich model [9]. Here we show that this formula is also a good approximation for $\gamma N \to \pi N$ amplitudes.

There exists very limited work on extracting the $\gamma N \to N^*$ transition form factors at resonance poles. The results reported in Ref. [15] are at the $Q^2 = 0$ photon point. To our knowledge, the Q^2 evolution of the $\gamma N \to N^*$ transition form factors at resonance poles have not been reported in the literature. All such information, such as the recent results of Refs. [16–18],

were obtained by using the the phenomenological parametrization of amplitudes with the Breit-Wigner form (simply called the Breit-Wigner parametrization in this article) to fit the data. We thus will explain in some detail the differences between our approach and these previous approaches. We find that although our Laurent expansion form is similar to the phenomenological Breit-Wigner parametrization, there are fundamental differences in defining the energy dependence of amplitudes and therefore there is no simple relation between the two approaches. The only comparison we can make is for the $\gamma N \to \Delta(1232)$ transition form factors if we follow the traditional practice to define that the Breit-Wigner resonance position of $\Delta(1232)$ is the energy where the real parts of the multipole amplitudes vanish. As is well recognized, the definition of the Breit-Wigner position becomes very model dependent at the higher-energy region where multichannels effects are important. We thus will not make comparisons with the previous results for the other two considered resonances in P_{11} and D_{13} partial waves.

In Sec. II, we will briefly review the analytic continuation method developed in Ref. [1] and explain how it is applied to evaluate the on-shell amplitudes of $\pi N, \gamma^* N \to \pi N$ transitions. Section III is devoted to explaining how the determined residues are used to extract the elasticity $\eta_{\rm el}$ of $N^* \to \pi N$ decay and the $\gamma^* N \to N^*$ transition form factors at resonance poles. The results for P_{11}, P_{33}, and D_{13} nucleon resonances are presented in Sec. IV. A summary is given in Sec. V.

II. ANALYTIC CONTINUATION METHOD

Within the formulation [4] for the EBAC-DCC model, the partial-wave amplitudes of meson-baryon reactions can be written as

$$T_{\beta,\alpha}(p', p; E) = t_{\beta,\alpha}(p', p; E) + t^R_{\beta,\alpha}(p', p; E), \tag{1}$$

where α, β represent the meson-baryon (MB) states γN, πN, ηN, ρN, σN, $\pi\Delta$, and

$$t^R_{\beta,\alpha}(p', p; E) = \sum_{i,j} \bar{\Gamma}_{\beta,i}(p'; E)[G_{N^*}(E)]_{i,j}\bar{\Gamma}_{\alpha,j}(p; E), \tag{2}$$

with

$$\left[G^{-1}_{N^*}\right]_{i,j}(E) = \left(E - m_{N^*_i}\right)\delta_{i,j} - \Sigma_{i,j}(E). \tag{3}$$

Here i, j denote the bare N^* states defined in the Hamiltonian. $m_{N^*_i}$ are their masses. The first term (called the meson-exchange amplitude from now on) in Eq. (1) is defined by the following coupled-channels equation

$$t_{\beta,\alpha}(p', p; E) = v_{\beta,\alpha}(p', p) + \int_C dq q^2 \sum_\gamma v_{\beta,\gamma}(p', q; E) \times G_\gamma(q, E) t_{\gamma,\alpha}(q, p; E), \tag{4}$$

where $v_{\beta,\alpha}$ is defined by meson-exchange mechanisms and $G_\gamma(q, E)$ is the propagator for channel γ. The dressed vertexes and the energy shifts of the second term in Eqs. (2) and (3) are defined by

$$\bar{\Gamma}_{\alpha,j}(p; E) = \Gamma_{\alpha,j}(p) + \int_C dq q^2 \sum_\gamma t_{\alpha,\gamma}(p', q; E) \times G_\gamma(q, E)\Gamma_{\gamma,j}(q), \tag{5}$$

$$\Sigma(E)_{i,j} = \int_C dq q^2 \sum_\gamma \Gamma_{\gamma,i}(q) G_\gamma(q, E)\bar{\Gamma}_{\gamma,j}(q), \tag{6}$$

where $\Gamma_{\alpha,i}(p)$ defines the coupling of the ith bare N^* state to channel α.

Because of the quadratic relation between energy E and momentum p there are two energy sheets for each two-body channel: the physical (unphysical) sheet is identified with $\mathrm{Im}(p) > (<)\ 0$ for the stable two-particle channels. Thus the scattering amplitudes of an n-channels model are defined on a Riemann energy sheet, which consists of 2^n sheets. For the EBAC-DCC model, defined by Eqs. (1) through (6), each sheet can be defined by the symbol $(z_{\pi N}, z_{\eta N}, z_{\pi\pi N}, z_{\pi\Delta}, z_{\rho N}, z_{\sigma N})$, where z_α can be p or u representing the physical or unphysical sheets of channel α. Note that an acceptable reaction model can only have bound state poles and unitarity cuts on the physical sheet $(pppppp)$. The sheets from all other possible combinations of u and p are called unphysical sheets on which the scattering amplitude can have poles. We are, however, only interested in poles that have large effects on scattering observables and therefore they must be on the sheets that are near the $(pppppp)$ physical sheet. These poles are called resonance poles and other poles are called shadow poles. It is known [19,20] that a shadow pole near the threshold of a channel can also have large effects on scattering observables and must also be considered in the search. As analyzed in Ref. [1] using several exactly soluble models, these poles are, in most cases, on sheets where the open (above threshold) MB channels are on unphysical u sheets and the closed (below threshold) channels are on the physical sheet. In the following we first recall how the analytic continuation method we developed in Ref. [1] is used to search for such resonance poles within the EBAC-DCC model. We then describe how it is used to extract the residues of the extracted resonance poles from on-shell amplitudes.

Since $v_{\alpha,\beta}$ and the bare vertex $\Gamma_{\alpha,i}$ are energy independent within the EBAC-DCC model, the analytic structure of the scattering amplitude defined previously as a function of E is mainly determined by the Green functions $G_\gamma(q, E)$. Thus the key for selecting the amplitude on the physical sheet or unphysical sheet is to take an appropriate path of momentum integration C in Eqs. (1) through (6) according to the locations of the singularities of the MB Green functions $G_\alpha(p, E)$ as E moves to the complex plane. This can be done independently for each MB channel. For a channel with stable particles such as πN and ηN, the MB Green function is

$$G_{\rm MB}(E, p) = \frac{1}{E - E_M(p) - E_B(p)}, \tag{7}$$

which has a pole at the on-shell momentum p_0 defined by

$$E = \sqrt{m_M^2 + p_0^2} + \sqrt{m_B^2 + p_0^2}. \tag{8}$$

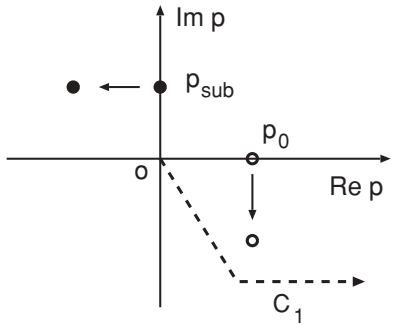

FIG. 1. The shift of the on-shell momentum (open circle/solid circle) of the two-particle Green function Eq. (7) as energy E moves from a real value above/below the threshold energy to a complex value with negative imaginary part. The C_1 (dotted line) is the integration path for calculating Eqs. (4)–(6) amplitude for E on the unphysical Riemann sheet.

As an example, let us consider the analytic continuation of the amplitude to the unphysical sheet of the MB channel when the energy E is above the threshold $\mathrm{Re}(E) > m_B + m_M$ and $\mathrm{Im}(E) < 0$. The on-shell momentum p_0 for such an E is on the second and the fourth quadrant of the complex momentum plane. As $\mathrm{Im}(E)$ becomes more negative as illustrated in Fig. 1, the on-shell momentum (open circle) moves into the fourth quadrant. The amplitude on the unphysical sheet can be obtained by deforming the path C into C_1 so that the on-shell momentum does not cross the integration contour. For energy below the threshold for the MB channel ($E < m_B + m_M$), the on-shell momentum p_{sub} is on the axis of positive-imaginary. As the energy moves into the region of $\mathrm{Re}(E) < m_B + m_M$ and $\mathrm{Im}(E) < 0$, p_{sub} moves to the second quadrant of the complex p plane and does not cross path C_1, as indicated by the dotted curves in Fig. 1. Hence the amplitudes on the physical sheet of the MB channel for energy below the MB threshold can also be obtained by taking the path C_1.

For the channels with an unstable particle such as $\pi\Delta$, as an example, the Green function is of the following form:

$$G_{\pi\Delta}(E,p) = \frac{1}{E - E_\pi(p) - E_\Delta(p) - \Sigma_\Delta(E,p)}, \qquad (9)$$

where

$$\Sigma_\Delta(p,E) = \int_{C_3} \frac{\{\Gamma_{\Delta,\pi N}(q)\}^2 q^2 dq}{E - E_\pi(p) - [(E_\pi(q) + E_N(q))^2 + p^2]^{1/2}}. \qquad (10)$$

The $\pi\Delta$ Green function in Eq. (9) has a singularity at momentum $p = p_x$, which satisfies

$$E - E_\pi(p_x) - E_\Delta(p_x) - \Sigma_\Delta(p_x,E) = 0. \qquad (11)$$

Physically, this singularity corresponds to the $\pi\Delta$ two-body "scattering state." There is also a discontinuity of the $\pi\Delta$ Green function associated with the $\pi\pi N$ cut in Σ_Δ, as shown in the dashed line in Fig. 2, where p_0 is defined by

$$E = E_\pi(p_0) + \left[(m_\pi + m_N)^2 + p_0^2\right]^{1/2}. \qquad (12)$$

Therefore, for $\mathrm{Re}(E) > m_B + m_M, 2m_\pi + m_N$, the integration contour C must be chosen to be below the $\pi\pi N$ cut

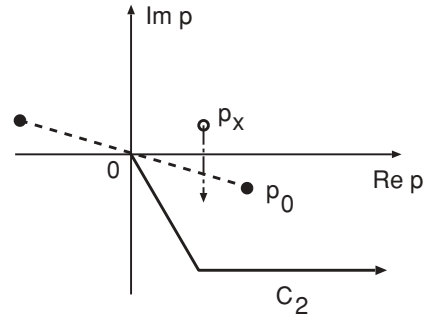

FIG. 2. Contour C_2 for calculating Eqs. (4)–(6) for E on the unphysical Riemann sheet with the unstable particle propagators, such as Eq. (9) for the $\pi\Delta$ channel. See the text for the explanations of the dashed line and the singularity p_x.

(dashed line) and the singularity p_x, such as the contour C_2 shown in Fig. 2, for calculating amplitudes on the unphysical sheet.

The singularity q_0 of the integrand of Eq. (10) depends on the spectator momentum p

$$E - E_\pi(p) = \{[E_\pi(q_0) + E_N(q_0)]^2 + p^2\}^{1/2}. \qquad (13)$$

Thus q_0 moves along the dashed curve, illustrated in Fig. 3, when the momentum p varies along the path C_2 of Fig. 2. To analytically continue $\Sigma_\Delta(p,E)$ to the unphysical sheet, the contour C_3 of Eq. (10) must be below q_0. A possible contour C_3 is the solid curve in Fig. 3.

We emphasize here that we can deform the contour C only in the region where the potential $v_{\alpha,\beta}(p',p)$ and the bare N^* vertex $\Gamma_{\mathrm{MB},N^*}(p)$ are analytic. The contours described previously are chosen only from considering the singularities of MB and the $\pi\pi N$ Green functions. Thus they must be further modified according to the analytic structure of the considered $v_{\alpha,\beta}(p',p)$ and $\Gamma_{\mathrm{MB},N^*}(p)$ to obtain the scattering amplitude in the momentum region of interest. This consideration is especially necessary when we need to get the on-shell amplitude for extracting the residues of the identified resonance poles. The residue of the amplitude at the resonance pole is evaluated from the "on-shell" matrix element, where the on-shell momenta are

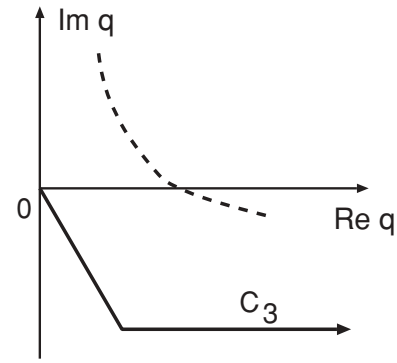

FIG. 3. Contour C_3 for calculating the Δ self-energy Eq. (10) on the unphysical Riemann sheet. Dashed curve is the singularity q_0 of the propagator in Eq. (13), which depends on the spectator momentum p on the contour C_2 of Fig. 2.

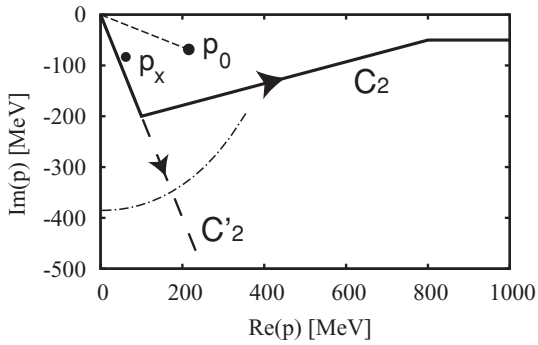

FIG. 4. The contour (solid curve) for calculating electromagnetic matrix element. p_0 and p_x are the singularities shown in Fig. 2. The dashed-dot curve is the singularity of the pion-exchange $\gamma N \to \pi\Delta$ matrix element at $E = (1357, -76i)$ MeV.

defined as $M_R = E_\pi(p^{\rm on}_{\pi N}) + E_N(p^{\rm on}_{\pi N})$ for the πN channel and $M_R = q^{0,\rm on}_{\gamma N} + E_N(q^{\rm on}_{\gamma N})$ with $(q^{0,\rm on}_{\gamma N})^2 = (q^{\rm on}_{\gamma N})^2 - Q^2$ for the $\gamma^* N$ channel. Here $Q^2 = -q^2 \geqslant 0$ is the four-momentum transfer square specified by the experiment. Since on-shell momentum are, in general, closer to the real axis than the momentum on contour C, the analytic properties of the meson-exchange potential has to be examined. For example, the t-channel meson exchange potential $v^t_{M'B',\rm MB}(\vec{p}\,',\vec{p})$ of the EBAC-DCC model has singularities at

$$\Delta^2 - (\vec{p} - \vec{p}')^2 = 0, \tag{14}$$

with $\Delta = E_{M'}(p') - E_M(p)$ or $E_{B'}(p') - E_B(p)$. The form of $\Gamma_{\rm MB,N^*}(p)$ is chosen such that its singularity is at the pure imaginary momentum. Thus the contours have to be chosen to also avoid these singularities. As an example, we show in Fig. 4 the singularities associated with the $\pi\Delta$ channel at $E = (1357, -76i)$ MeV. The dotted line for the $\pi\pi N$ cut and the circle shows p_X are the singularities from the Green's function, as discussed previously. The most relevant singularity of the meson-exchange potential in our investigation of electromagnetic pion production amplitude is due to the t-channel pion exchange of $\gamma N \to \pi\Delta$, which is shown as the dashed-dot curve. Thus the integration contour has to be modified to the solid curve C_2 in Fig. 4. This can be understood from Fig. 5 in which we see that the matrix element (dashed curves) of the nonresonant potential $v_{\pi\Delta,\gamma N}$ encounters the cut around $\mathrm{Re}(p) \sim 170$ MeV with the path C_2', but it varies smoothly (solid curves) along the path C_2.

III. EXTRACTION OF TRANSITION FORM FACTORS

To indicate the essential features of our approach more clearly, it is useful to first briefly describe how the resonance parameters are defined in the previous investigations. The scattering amplitude $F_{\beta,\alpha}$ between any two channels α and β is related to the S-matrix element by $F_{\beta,\alpha} = (S_{\beta,\alpha} - 1)/2i$. Within the rather general theoretical framework discussed by, for example, Dalitz and Moorhouse [13], Taylor [21], and McVoy [22], $F_{\beta,\alpha}$ at energies near a resonance pole position M_R is parametrized as a sum of a pole term and a constant nonresonant contribution

$$F_{\beta,\alpha}(E \to M_R) \sim \frac{R_{\beta,\alpha}}{M_R - E} + B_{\beta,\alpha}, \tag{15}$$

where $R_{\beta,\alpha}$ is the residue at the pole position M_R and the nonresonant amplitude $B_{\beta,\alpha}$ is an energy-independent complex number. By the unitarity condition imposed on the full S matrix $F_{\alpha,\beta}(E)$ at $E \to M_R$, the nonresonant term $B_{\alpha,\beta}$ is written in terms of a nonresonant S matrix S^B, which is unitary by itself $(S^B S^{B\dagger} = 1)$

$$B_{\beta,\alpha} = \frac{S^B_{\beta,\alpha} - 1}{2i}. \tag{16}$$

Then the pole term of Eq. (15) is defined by the partial width Γ_α and a phase ϕ_α arising from the presence of the nonresonant term $B_{\alpha,\beta}$

$$\frac{R_{\beta,\alpha}}{E - E_R} = \frac{e^{i\phi_\beta}\sqrt{\Gamma_\beta/2}\,e^{i\phi_\alpha}\sqrt{\Gamma_\alpha/2}}{E - M_R}. \tag{17}$$

It is important to note that for the $\gamma N \to \pi N$ amplitudes we are going to consider, $e^{i\phi_{\gamma N}}\sqrt{\Gamma_{\gamma N}}$ is the electromagnetic $\gamma N \to N^*$ form factor which clearly must be a complex number when the the nonresonant term $B_{\pi N,\gamma N}$ is present and $\phi_{\gamma N} \neq 0$. We will see that our formulas are consistent with these earlier investigations and will yield complex $\gamma N \to N^*$ form factors. Our main advance is to provide their interpretations in terms of the dynamics defined within the EBAC-DCC model.

Here we mention that by introducing the appropriate energy-dependence of $\mathrm{Im}(M_R)$, $R_{\alpha\beta}$, and $B_{\alpha,\beta}$, the expression

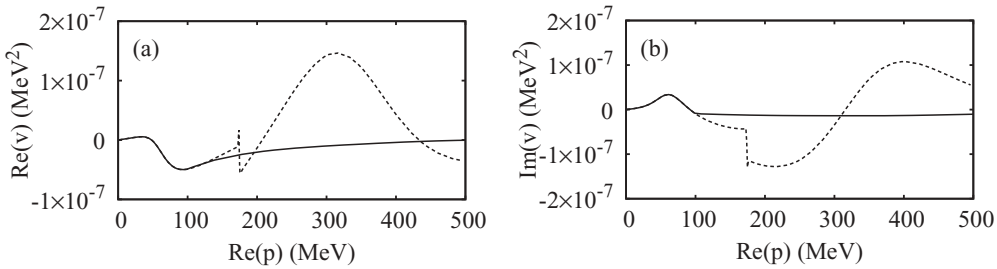

FIG. 5. The real (left) and the imaginary (right) parts of the half-off-shell matrix-elements of the nonresonant potential $v_{\gamma N\to\pi\Delta}$ for P_{11} partial wave at $E = (1357, -76i)$, as functions of the real part [Re(p)] of off-shell momentum. The solid (dashed) curve is from the calculation along the path C_2 (C_2') shown in Fig. 4.

Eq. (15) is used in practice to fit the experimental data. This is the origin of the commonly used Breit-Wigner parametrization of the amplitude in the physical energy region. In some recent analyses [16–18] based on such a Breit-Wigner parametrization, the extracted $\gamma^* N \to N^*$ form factors are reported as real numbers. Clearly, this is rather different from what one can interpret from the previous formula used in the earlier analyses [13,21,22]. We will discuss this issue further in Sec. IV.

We now explain that within the EBAC-DCC model, it is straightforward to extract the resonance parameters M_R, $B_{\alpha,\beta}$, and $R_{\alpha,\beta}$ of Eq. (15) by performing a Laurent expansion of the T matrix defined in Eqs. (1) through (6). We need to find the poles of the scattering amplitudes $T_{\alpha,\beta}$. In principle, the pole of the scattering amplitude can be found in the meson-exchange amplitude t and/or the resonance amplitude t^R of Eq. (1). However, as pointed out in Ref. [14], a pole M_x of the meson-exchange amplitude t does not survive as a pole of the full amplitude when we introduce coupling with bare N^* states since there is an exact cancellation between the pole contributions from t and t^R at $E = M_x$. Furthermore, the nonresonant term at resonance pole $t(E = M_R)$ is finite. Thus, the resonance poles of EBAC-DCC, or any model with bare N^* states, can be found by only analyzing t^R defined by Eq. (2). Consequently, we only need to explain how the residues of the resonance poles are extracted from the term t^R.

The pole positions M_R of t^R are found from the zeros of the determinant of the N^* propagator defined by Eq. (3)

$$\Delta(E = M_R) = \det\left[G^{-1}_{N^*}(E = M_R)\right] = 0. \tag{18}$$

The pole term of the N^* Green function can be expressed as

$$[G_{N^*}(E)]_{ij} = \frac{\chi_i \chi_j}{E - M_R}, \tag{19}$$

where i, j denote the bare N^* state in the free Hamiltonian and χ_i represents the ith "bare" resonance component of the dressed N^* and satisfies

$$\sum_j [G_{N^*}(M_R)^{-1}]_{ij}\chi_j = \sum_j \left[(M_R - m_{N^*_i})\delta_{ij} - \Sigma(M_R)_{ij}\right]\chi_j = 0. \tag{20}$$

If there is only one bare N^* state, with $G^{-1}_{N^*}(E) = 1/[E - m_{N^*} - \Sigma(E)]$, it is easy to see that

$$\chi = \frac{1}{\sqrt{1 - \Sigma'(M_R)}}, \tag{21}$$

where $\Sigma'(M_R) = [d\Sigma/dE]_{E=M_R}$. If we have two bare N^* states, Eq. (20) leads to

$$\chi_1 = \sqrt{\frac{M_R - m_{N^*_2} - \Sigma_{22}(M_R)}{\Delta'(M_R)}}, \tag{22}$$

$$\chi_2 = \frac{\Sigma_{12}(M_R)}{M_R - m_{N^*_2} - \Sigma_{22}(M_R)}\chi_1, \tag{23}$$

where $\Delta'(M_R) = [d\Delta/dE]_{E=M_R}$ can be evaluated using Eq. (18).

Now it is straightforward to see how the residues $R_{\beta,\alpha}$ and the nonresonant term $B_{\beta,\alpha}$ of Eq. (15) can be extracted from the amplitude $T_{\beta,\alpha}$ defined by Eq. (1). First we note that at E near the resonance pole M_R, the full amplitude defined by Eq. (1) can be written as

$$T_{\beta,\alpha}\left(p^{\rm on}_\beta, p^{\rm on}_\alpha; E \to M_R\right) = t_{\beta,\alpha}\left(p^{\rm on}_\beta, p^{\rm on}_\alpha; M_R\right) + t^R_{\beta,\alpha}\left(p^{\rm on}_\beta, p^{\rm on}_\alpha; E \to M_R\right), \tag{24}$$

where $p^{\rm on}_\alpha$ is the on-shell momentum of channel α [e.g., $M_R = E_\pi(p^{\rm on}_{\pi N}) + E_N(p^{\rm on}_{\pi N})$ for the πN channel] and $t_{\beta,\alpha}(p^{\rm on}, p^{\rm on}; M_R)$ is finite, as explained previously. By using Eq. (2) for the definition of $t^R_{\beta,\alpha}$ and Eq. (19) for the pole term of the N^* propagator, we can perform the Laurent expansion of the on-shell element of Eq. (24) to obtain

$$T_{\beta,\alpha}\left(p^{\rm on}_\beta, p^{\rm on}_\alpha; E \to M_R\right) = \frac{\bar\Gamma^R_\beta \bar\Gamma^R_\alpha}{E - M_R} + B_{\beta,\alpha} + B^1_{\beta,\alpha}(E - M_R) + \cdots, \tag{25}$$

where

$$\bar\Gamma^R_\alpha = \sum_j \chi_j \bar\Gamma_{\alpha,j}\left(p^{\rm on}_\alpha, M_R\right). \tag{26}$$

Here the dressed vertex $\bar\Gamma_{\alpha,j}$ is defined by Eq. (5). The terms $B_{\beta,\alpha}$ and $B^1_{\beta,\alpha}$ in Eq. (25) depend on the matrix elements of the meson-exchange amplitude t of Eq. (1)

$$B_{\beta,\alpha} = t_{\beta,\alpha}\left(p^{\rm on}_\beta, p^{\rm on}_\alpha; M_R\right) + \frac{d}{dE}\left[(E - M_R)t^R_{\beta,\alpha}\left(p^{\rm on}_\beta, p^{\rm on}_\alpha; E\right)\right]_{E=M_R}. \tag{27}$$

The term $B^1_{\beta,\alpha}$ can be calculated, but is not relevant to our following discussions.

Let us now consider Eq. (25) for the $\alpha = \beta = \pi N$ case. We need to relate the residue $\bar\Gamma_{\pi N}\bar\Gamma_{\pi N}$ of its pole term to the residue of the πN elastic scattering amplitude $F_{\pi N,\pi N}$ defined by the standard notation

$$F_{\pi N,\pi N}(E \to M_R) = \left[\frac{S_{\pi N,\pi N}(E) - 1}{2i}\right]_{E\to M_R} = \left[\frac{{\rm Re}^{i\phi}}{M_R - E}\right]_{E\to M_R}, \tag{28}$$

where $S_{\pi N,\pi N}$ is the partial-wave S matrix. In terms of the normalization of the EBAC-DCC model $S_{\pi N,\pi N}(E) = 1 - 2i[\pi p^{\rm on} E_\pi(p^{\rm on})E_N(p^{\rm on})/E]T_{\pi N,\pi N}(p^{\rm on}, p^{\rm on}; E)$, we find that ($p^{\rm on}$ stands for $p^{\rm on}_{\pi N}$)

$$F_{\pi N,\pi N}(M_R) = -\pi\frac{p^{\rm on}E_N(p^{\rm on})E_\pi(p^{\rm on})}{M_R}T_{\pi N,\pi N}(p^{\rm on}, p^{\rm on}, M_R). \tag{29}$$

Keeping only the pole term of Eq. (25) in evaluating the above equation and using the definition Eq. (28), we then obtain

$${\rm Re}^{i\phi} = \pi\frac{p^{\rm on}E_N(p^{\rm on})E_\pi(p^{\rm on})}{M_R}\bar\Gamma^R_{\pi N}\bar\Gamma^R_{\pi N}. \tag{30}$$

The πN elasticity of a resonance is then defined as

$$\eta_e = \frac{R}{-{\rm Im}(M_R)}. \tag{31}$$

TABLE I. The extracted resonance poles ($\mathrm{Re}M_R$, $-\mathrm{Im}M_R$) MeV and elasticity η_e [Eq. (31)] are compared with the values listed by PDG [23].

	M_R (EBAC-DCC)	location	M_R (PDG)	η_e (EBAC-DCC)	η_e (PDG)
P_{33}	(1211,50)	(u-ppp-)	(1209–1211, 49–51)	100%	100%
D_{13}	(1521,58)	($uuuupp$)	(1505–1515, 52–60)	65%	55–65%
P_{11}	(1357,76)	($upuupp$)	(1350–1380, 80–110)	49%	55–75%
	(1364,105)	($upuppp$)		60%	
	(1820,248)	($uuuuup$)	(1670–1770, 40–190)	8%	10–20%

With the similar procedure, we can perform the Laurent expansion of the $\gamma^*N \to \pi N$ amplitude to obtain

$$T_{\pi N,\gamma N}(p^{\mathrm{on}}, q^{\mathrm{on}}; E \to M_R) = \frac{\bar{\Gamma}^R_{\pi N}(p^{\mathrm{on}})\bar{\Gamma}^R_{\gamma N}(q^{\mathrm{on}}, Q^2)}{E - M_R} + B_{\pi N,\gamma N} + \cdots, \quad (32)$$

where q^{on} stands for $q^{\mathrm{on}}_{\gamma N}$. As discussed in Sec. I, a nucleon resonance can be interpreted [12,13] as an "eigenstate" of the Hamiltonian $H|\psi^R_{N^*}\rangle = M_R|\psi^R_{N^*}\rangle$. Then from the spectral expansion of the Low equation for reaction amplitude $T(E) = H' + H'\frac{1}{E-H}H'$, where we defined $H' = H - H_0$ with H_0 being the noninteracting free Hamiltonian, we have

$$T_{\pi N,\gamma N}(p^{\mathrm{on}}, q^{\mathrm{on}}; E \to M_R) = \frac{\langle p^{\mathrm{on}}|H'|\psi^R_{N^*}\rangle\langle\psi^R_{N^*}|H'|q^{\mathrm{on}}, Q^2\rangle}{E - M_R} + \cdots. \quad (33)$$

Obviously, we can see that $\langle\psi^R_{N^*}|H'|q^{\mathrm{on}}, Q^2\rangle = \langle\psi^R_{N^*}|J^\mu(Q^2)\epsilon_\mu|N\rangle$ is determined by the electromagnetic current operator $J^\mu(Q^2)$. It must be a complex number since the resonance wave function $\psi^R_{N^*}$ contains scattering states. Comparing Eqs. (32) and (33), we then interpret $\bar{\Gamma}^R_{\gamma N}(q^{\mathrm{on}}, Q^2)$ as the $N^*_R \to \gamma^*N$ transition form factor. As seen in Eq. (19), the resonance consists of all bare N^* components and hence we have

$$\langle\psi^R_{N^*}|J^\mu(Q^2)\epsilon_\mu|N\rangle = \sum_i \chi_i \bar{\Gamma}_{\gamma N,N^*_i}(q^{\mathrm{on}}, Q^2). \quad (34)$$

Using the normalizations defined in Ref. [11] and following the definition originally introduced for the constituent quark model [24], the usual $\gamma^*N \to N^*$ transition form factors are related to our extracted from factors by

$$A_{3/2}(Q^2) = C\sum_j \chi_j \bar{\Gamma}^R_{\gamma^*N,j}(Q^2, M_R, \lambda_\gamma = 1, \lambda_N = -1/2), \quad (35)$$

$$A_{1/2}(Q^2) = C\sum_j \chi_j \bar{\Gamma}^R_{\gamma^*N,j}(Q^2, M_R, \lambda_\gamma = 1, \lambda_N = 1/2), \quad (36)$$

$$S_{1/2}(Q^2) = C\sum_j \chi_j \bar{\Gamma}^R_{\gamma^*N,j}(Q^2, M_R, \lambda_\gamma = 0, \lambda_N = -1/2), \quad (37)$$

where λ_N and λ_γ are the helicities of the initial nucleon and photon, respectively, and

$$C = \sqrt{\frac{E_N(\vec{q})}{m_N}}\frac{1}{\sqrt{2K}} \times \sqrt{\frac{(2j+1)(2\pi)^3(2q_0)}{4\pi}}, \quad (38)$$

where $K = (M_R^2 - m_N^2)/(2M_R)$. The above formulas are derived by using the formula detailed in Ref. [7] for relating the $\gamma^*N \to N^*$ form factor to multipole amplitudes.

IV. RESULTS AND DISCUSSION

In this section, we illustrate our procedures by presenting the results for the pronounced resonances in P_{33}, D_{13}, and the complex P_{11} partial waves. We also investigate the extent to which our results can be compared with those extracted from using the Breit-Wigner form of resonant amplitudes to fit the data.

Before we present our results for the electromagnetic form factors, it is useful to first discuss our results from the πN scattering amplitudes, which were briefly presented in Refs. [1,2]. The extracted pole positions (M_R) and elasticities η_e defined by Eq. (31) for P_{33}, D_{13}, and P_{11} are compared with the values from the Particle Data Group (PDG) [23] in Table I. We see that our results correspond well with PDG, while only one P_{11} near 1360 MeV is listed by PDG [23]. The extracted residues $\mathrm{Re}^{i\phi}$, defined in Eq. (30), for the πN amplitude are compared with some of the previous work in Table II. We see

TABLE II. The extracted πN residues $\mathrm{Re}^{i\phi}$ defined by Eq. (30) are compared with several previous results.

	EBAC-DCC		GWU-VPI [16]		Cutkosky [26]		Jülich [14]	
	R	ϕ	R	ϕ	R	ϕ	R	ϕ
$P_{33}(1211)$	52	−46	52	−47	53	−47	47	−37
$D_{13}(1521)$	38	7	38	−5	35	−12	32	−18
$P_{11}(1357)$	37	−111	38	−98	52	−100	48	−64
(1364)	64	−99	86	−46	–	–	–	–
(1820)	20	−168	–	–	9	−167	–	–

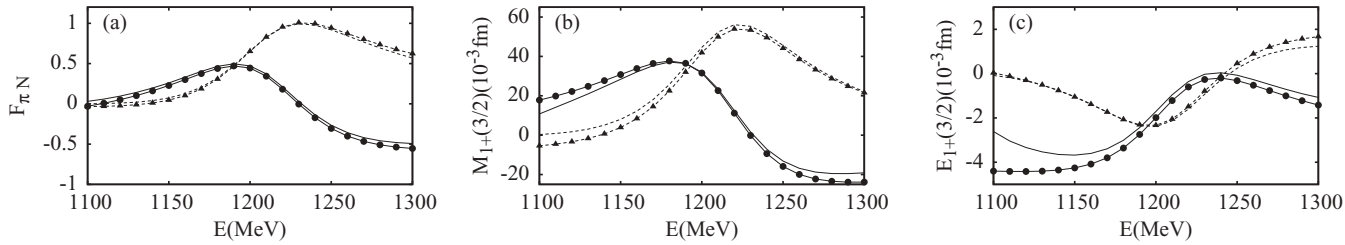

FIG. 6. Energy dependence of (a) the πN amplitude and (b) the $\gamma\pi$ $M_{1+}(3/2)$ and (c) $E_{1+}(3/2)$ amplitudes of the P_{33} channel. The solid circle (triangle) shows the real (imaginary) part of the amplitude calculated using Eq. (15). The solid (dashed) curve shows the real (imaginary) part of the amplitude of the EBC-DCC model.

that the agreement in P_{33} and D_{13} is excellent. However, we see that the residues of the P_{11} resonances extracted by four groups do not agree well while we agree well with GWU/VPI only for the resonance at 1356 MeV.

In Table I, we also indicate the location of each pole on the Riemann energy sheet. Since we only search for poles in the region where the open (above threshold) channels are on the unphysical u sheet and the close channels (below threshold) on the physical p sheets, as described in Sec. II, the quantity deciding which sheet each resonance in Table I is on are the branching points for each channel, Within the JLMS fit they are $(1077, 1486, 1216, 1363 - 33i, 1703 - 75i, 1906 - 323i)$ MeV for $(\pi N, \eta N, \pi\pi N, \pi\Delta, \rho N, \sigma N)$, respectively. For example, the P_{11} pole at 1357 MeV(1364 MeV) is below (above) the $\pi\Delta$ threshold 1363 MeV and is on $upuupp$ ($upuppp$) sheets since both poles are above the πN and $\pi\pi N$ channels and below the ηN, ρN, and σN channels. Thus their residues are very different although their positions are very close since they are on different Riemann sheets. This two-poles structure near the $\pi\Delta$ threshold is also found in the earlier analysis of VPI [25] and Cutkosky and Wang [26], and the recent analysis by the GWU/VPI [16] and Jülich [14] groups.

Our results presented in Tables I and II suggest that the resonance parameters of the pronounced and well-isolated resonance poles, such as $P_{33}(1210)$ and $D_{13}(1521)$, are rather safely determined by the structure of the empirical partial-wave amplitudes as long as the employed models have the correct analytic properties in the region not far from the physical region. On the other hand, the residues of the poles near threshold are sensitive to the dynamical content of the models, as we saw in the considered P_{11} case.

We now turn to presenting our results for the $\gamma^* N \to N^*$ form factors $A_\lambda(Q^2)$ and $S_\lambda(Q^2)$. We first observe that for the isolated resonances in P_{33} and D_{13}, Eqs. (25) and (27) for $\gamma^* N \to \pi N$ multipole amplitudes at $E \to M_R$ can be approximated as the following simple form:

$$T_{\pi N,\gamma N}(E \to M_R) = B_{\pi N,\gamma N} - \frac{R_{\pi N,\gamma N}}{E - M_R}, \tag{39}$$

where the complex constants are evaluated at resonance position $E = M_R$

$$B_{\pi N,\gamma N} = t_{\pi N,\gamma N}(p^{\text{on}}, q^{\text{on}}; M_R) + \frac{d}{dE}\left[(E - M_R) t^R_{\pi N,\gamma N}(p^{\text{on}}, q^{\text{on}}; E)\right]_{E=M_R}, \tag{40}$$

$$R_{\pi N,\gamma N} = -\bar{\Gamma}^R_{\pi N}(p^{\text{on}}, M_R) A_\lambda(Q^2, M_R)/C. \tag{41}$$

Here C is defined by Eq. (38). We observe that the expression in Eq. (39), evaluated with all constants except E kept at their complex values at pole position M_R, is a good approximation in the physical region of E near $W_R = \text{Re}(M_R)$. A similar, good approximation is also for the $\pi N \to \pi N$ amplitudes, as also reported in Ref. [14]. Our findings are shown in Figs. 6 and 7 for the P_{33} and D_{13} partial waves, respectively. The determined constants $B_{\pi N,\gamma^* N}$, $R_{\pi N,\gamma N}$, $B_{\pi N,\pi N}$ $R_{\pi N,\pi N}$, and M_R for each case in Figs. 6 and 7 are presented in Table III.

We now note that the Laurent expansion expression in Eq. (39) looks similar to the commonly used amplitude with a Breit-Wigner parametrization

$$T^{\text{BW}}_{\pi N,\gamma N}(E) = B_{\pi N,\gamma^* N}(Q^2; E) + \frac{\Gamma^{1/2}_{\pi N}(E) e^{i\phi^{\text{BW}}(E)} A^{\text{BW}}_\lambda(Q^2, E)}{E - \left(W_R - i\frac{\Gamma_{\text{tot}}(E)}{2}\right)}, \tag{42}$$

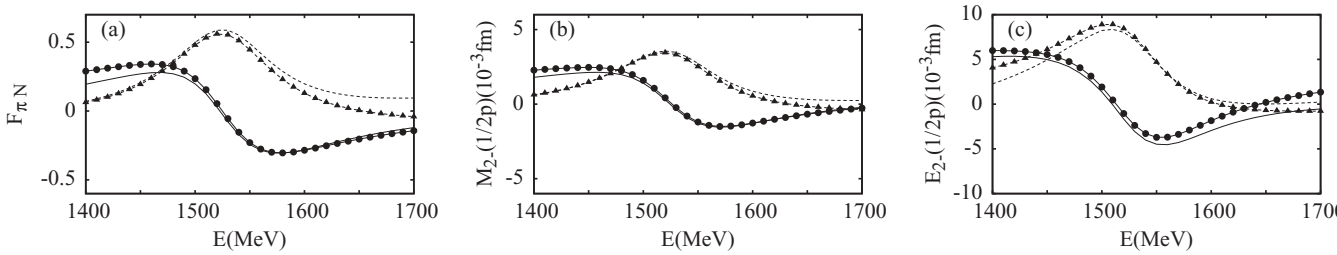

FIG. 7. Energy dependence of the (a) πN amplitude and (b) the $\gamma\pi$ $M_{2-}(1/2p)$ and (c) $E_{2-}(1/2p)$ amplitudes of the D_{13} channel. The solid circle (triangle) shows the real (imaginary) part of the amplitude calculated using Eq. (15). The solid (dashed) curve shows the real (imaginary) part of the amplitude of the EBC-DCC model.

TABLE III. Extracted resonance parameters. $R_{\beta,\alpha}$ and $B_{\beta,\alpha}$ are for the πN elastic scattering amplitude $F_{\pi N,\pi N}$ and multipole amplitudes $E_{L\pm}$, $M_{L\pm}$ of the pion photoproduction.

	M_R(MeV)	$R_{\pi N,\pi N}$(MeV)	$B_{\pi N,\pi N}$		$R_{\pi N,\gamma N}(10^{-3}$ fm MeV)	$B_{\pi N,\gamma N}(10^{-3}$ fm)
P_{33}	$1211-50i$	$36.1-37.7i$	$-0.43+0.13i$	$M_{1+}(3/2)$	$-2728+1436i$	$-7.43-3.86i$
				$E_{1+}(3/2)$	$175+118i$	$-3.49+1.51i$
D_{13}	$1521-58i$	$37.6+4.9i$	$0.06-0.08i$	$M_{2-}(1/2p)$	$-224-61.6i$	$1.01-0.44i$
				$E_{2-}(1/2p)$	$-437-368i$	$4.25+0.36i$

where $\Gamma_{\rm tot}(E=W_R)$ and $\Gamma_{\pi N}(E=W_R)$ are called the total width and partial decay width for the πN channel, respectively, and $A_\lambda^{\rm BW}(Q^2,q,E)$ is assumed to be real numbers. The energy dependence of these widths as well as the phase factor $\phi^{\rm BW}(E)$ are parts of the assumptions in those analysis, which, of course, will influence how the nonresonant amplitude $B_{\pi N,\gamma^*N}(Q^2;E)$ is adjusted to fit the data.

Equations (39) and (42) have a similar structure, but they have important differences. First the Laurent expansion expression of Eq. (39) is evaluated at complex M_R and hence the on-shell momentum $q^{\rm on}$ and $p^{\rm on}$ are also complex. However, all the energy and momentum variables in Eq. (42) are real numbers defined by the physical energy E. The nonresonant amplitude $B_{\pi N,\gamma N}$ in Eq. (39) is obtained from a coupled-channel calculation based on the equations presented in Sec. II, while $B_{\pi N,\gamma^*N}(Q^2;E)$ in Eq. (42) is often calculated from tree-diagrams of the phenomenological Lagrangian with unitarization using the πN amplitude. Clearly, there is no simple relation between these two approaches. We thus will not make comparisons of our results at resonance pole positions with those extracted from using the Breit-Wigner parametrization Eq. (42). This important difference must be clarified further in the future to know how these two different extracted resonance parameters can be used meaningfully to test hadron structure calculations.

The two-pole structure of P_{11} resonances near the $\pi\Delta$ threshold poses a problem in interpreting our results for the $\gamma^*N\to N^*$ form factors $A_\lambda(Q^2)$. We note that Eq. (39) is valid for each of these two poles, but they are on different Riemann surfaces. Thus we need to find a parametrization that carries the sheet information in representing these two-pole contributions. Here we follow the approach of Refs. [27–29] and a similar formula used in extracting meson resonances [20,30].

We first use Eq. (39) to write the $\pi N\to\pi N$ and $\gamma N\to\pi N$ scattering amplitudes on the $\pi\Delta$ physical ($a=p$) and unphysical ($a=u$) sheet as

$$T^{(a)}_{\beta,\alpha}\left(p^{\rm on}_\beta,p^{\rm on}_\alpha,E\to M^{(a)}_R\right)=-\frac{R^{(a)}_{\beta,\alpha}}{E-M^{(a)}_R}+B^{(a)}_{\beta,\alpha},\qquad(43)$$

where α,β represent the πN or γN channels. All parameters $R^{(a)}_{\beta,\alpha}$, $B^{(a)}_{\beta,\alpha}$, and $M^{(a)}_R$ are obtained numerically from the amplitude as described in the previous section. The above two amplitudes with $a=u,p$ can be combined by using the following unified representation:

$$T_{\beta,\alpha}\left(p^{\rm on}_\beta,p^{\rm on}_\alpha,E\to M_R\right)=-\frac{R_{\beta,\alpha}+R^1_{\beta,\alpha}p_{\pi\Delta}}{E-M_R-\gamma p_{\pi\Delta}}+B_{\beta,\alpha}+B^1_{\beta,\alpha}p_{\pi\Delta},\qquad(44)$$

where $p_{\pi\Delta}$ is the $\pi\Delta$ on-shell momentum p_x determined by Eq. (11). We require $T_{\beta,\alpha}=T^{(p/u)}_{\beta,\alpha}$ at $p_{\pi\Delta}=p^{(p/u)}_{\pi\Delta}$. This requirement for $\alpha=\pi N,\gamma N$ and $\beta=\pi N$ determines six unknown complex numbers R, R^1, M_R, B, B^1, and γ from the known parameters $R^{(a)}_{\beta,\alpha}$, $B^{(a)}_{\beta,\alpha}$, and $M^{(a)}_R$. Neglecting the small contribution of R^1 and B^1, we then obtain

$$T_{\beta,\alpha}\left(p^{\rm on}_\beta,p^{\rm on}_\alpha,E\to M_R\right)=-\frac{R_{\beta,\alpha}}{E-M_R-\gamma p_{\pi\Delta}}+B_{\beta,\alpha},\qquad(45)$$

where

$$\gamma=\frac{M^{(p)}_R-M^{(u)}_R}{p^{(p)}_{\pi\Delta}-p^{(u)}_{\pi\Delta}},\qquad(46)$$

$$M_R=M^{(p)}_R-\gamma p^{(p)}_{\pi\Delta},\qquad(47)$$

$$R^1_{\beta,\alpha}=\frac{R^{(p)}_{\beta,\alpha}\left(1-\gamma dp^{(p)}_{\pi\Delta}/dE\right)-R^{(u)}_{\beta,\alpha}\left(1-\gamma dp^{(u)}_{\pi\Delta}/dE\right)}{p^{(p)}_{\pi\Delta}-p^{(u)}_{\pi\Delta}},\qquad(48)$$

$$R_{\beta,\alpha}=R^{(p)}_{\beta,\alpha}\left(1-\gamma dp^{(p)}_{\pi\Delta}/dE\right)-p^{(p)}_{\pi\Delta}R^1_{\beta,\alpha}.\qquad(49)$$

With $p^{(u)}_{\pi\Delta}=49-68i$ MeV, $M^{(u)}_R=(1359-76i)$ MeV, and $p^{(p)}_{\pi\Delta}=-65+86i$ MeV, $M^{(p)}_R=(1357-76i)$ MeV, we have $M_R=(1364-105i)$MeV, $\gamma=-0.146+0.062i$ and $R_{\pi N,\pi N}=(-12-47i)$MeV. The quantities $R^{(u/p)}_{\pi N,\gamma N}$ at Q^2 can be obtained from $\bar\Gamma^R_{\pi N}\bar\Gamma^R_{\gamma N}$ of Eq. (39) and hence $R_{\pi N,\gamma N}$ can also be calculated from using Eqs. (46) through (49). By interpreting $R_{\pi N,\pi N}$ and $R_{\pi N,\gamma N}$ of Eq. (45) as the residues of a pole and using the procedures described previously, we can then extract the electromagnetic helicity amplitudes $A_\lambda(Q^2)$ and $S_\lambda(Q^2)$.

We found that the unified formula Eq. (45) is a good approximation for both the πN and $\gamma\pi$ amplitudes if Eq. (43) is evaluated in the physical region where E is near $W_R=$ Re(M_R). This is shown in Fig. 8 for the considered P_{11} partial wave. Although Eq. (45) is close to the commonly used Breit-Wigner form of Eq. (42), we will not compare the extracted $\gamma^*N\to N^*$ helicity amplitude $A_\lambda(Q^2)$ with those from the previous analysis using the Breit-Wigner parametrization, for the same reasons discussed previously for the isolated P_{33} and D_{13} resonances.

We now turn to presenting our results for the $\gamma^*N\to N^*$ form factors for the P_{33}, D_{13}, and P_{11} resonances at the $Q^2=0$ photon point. The electromagnetic parameters for calculating the pion photoproduction amplitudes within EBAC-DCC were determined in Ref. [10]. Our results at the resonance poles are listed in Table IV. We see that in most cases, their

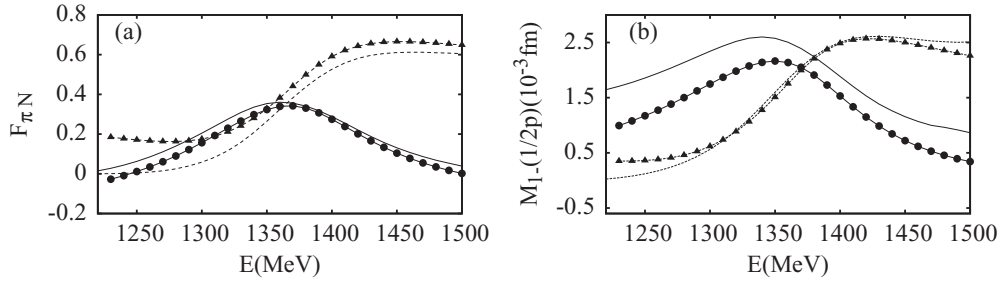

FIG. 8. Energy dependence of (a) the $P_{11}\pi N$ scattering and (b) the $M_{1-}(1/2p)\ \gamma\pi$ amplitude. The solid circle (triangle) shows the real (imaginary) part of the amplitude calculated using Eq. (45). The solid (dashed) curve shows the real (imaginary) part of the amplitude of the EBC-DCC model.

imaginary parts are sizable. As discussed previously, they have no simple relation with those extracted from using the Breit-Wigner parametrization. The only comparison we can make is for the $\gamma N \to \Delta(1232)$ transition form factors if we follow the traditional practice to define that the Breit-Wigner resonance position of $\Delta(1232)$ is the energy $E = 1232$ MeV where the real parts of the multipole amplitudes vanish. By using the procedure described in Ref. [7], our results for this Breit-Wigner position are listed in the third column of Table V. We see that our results are in good agreement with the previous results [31–34] from using the Breit-Wigner parametrization. It has been well recognized that the definition of the Breit-Wigner position has become very model dependent in the higher-energy region where multichannels effects are important. We thus do not make comparisons for the other two considered resonances in P_{11} and D_{13} partial waves.

We now present the Q^2 evolution of the extracted $\gamma^* N \to N^*$ form factors. The pion electroproduction amplitudes are calculated using the parameters determined from fitting [11] the CEBAF Large Acceptance Spectrometer (CLAS) $p(e, e'\pi)$ data [18,35–37] at several Q^2. As discussed in Ref. [11], we fit the data by adjusting only the bare helicity amplitudes of the EBAC-DCC model. Because the quality of the data at each Q^2 is different (as summarized in Table I of Ref. [11]), our determined bare helicity amplitudes are not a smooth function of Q^2. Consequently, the extracted helicity amplitudes at resonance poles are not a smooth function of Q^2. It is not a simple task to specify the errors for the extracted resonance parameters at resonance poles. Since the objective of this article is mainly to explain our resonance extraction procedure, we thus will not resolve this problem. This important issue, however, must be dealt with in the future. Here we mention that most, if not all, of the previous work on resonance information at resonance poles, such as those listed in Table II, have not given errors.

For P_{33} we can use the standard relation [7] to evaluate the N-Δ magnetic transition form factor G_M^* in terms of helicity amplitudes. Our results are shown in the left side of Fig. 9. The real and imaginary parts of the extracted $G_M^*(Q^2)$ are the solid circles (connected by the solid curves) and triangles (connected by the dotted line), respectively. As mentioned previously, these results at resonance pole $M_R = 1210 - 50i$ cannot be meaningfully compared with the previous results extracted from using the Breit-Wigner parametrization. It is only meaningful to compare our results at Briet-Wigner position $W = 1232$ MeV with those of the earlier results. This comparison is also shown in the right side of Fig. 9. We see that our results at Briet-Wigner position $E = 1232$ MeV (open squares connected by dashed curve) are in good agreement with the results (solid circles with errors) from the previous analysis [18,38–40] using the Breit-Wigner parametrization.

Our results for the resonance pole of D_{13} and the three poles of P_{11} listed in Table I are shown in Figs. 10 and 11, respectively. Similar to the results at the photon point presented in Table IV, their imaginary parts (solid triangles) are comparable or larger than the real parts (solid circles) in magnitudes. We note that the Q^2 dependence of the helicity amplitudes for P_{11} in Fig. 11 indicates that the structure of the first two poles $N^*(1356)$ and $N^*(1364)$ is quite different from the third $N^*(1820)$.

For the P_{11} case, it is perhaps more appropriate to interpret our results calculated from using the unified form Eq. (43) for the two poles near the $\pi\Delta$ threshold as the values that can be identified with the Roper $N^*(1440)$ resonance listed by PDG. This results are shown in Fig. 12. We again see that its imaginary parts (dotted line) are comparable or larger than its real parts (solid line) in most of the Q^2 region. Here we also see that the contribution (dot-dashed lines) from the determined bare $\gamma N \to N^*$ strengths play an important role in

TABLE IV. The extracted $\gamma N \to N^*$ helicity amplitudes (A_λ in 10^{-3} GeV$^{-1/2}$) at nucleon pole positions. The values for $P11$(total) are from using Eq. (45), which gives a unified representation of the results from two poles at $(1356 - 76i)$ and $(1364 - 105i)$ near the $\pi\Delta$ threshold.

	$P_{33}(1210 - 50i)$	$D_{13}(1521 - 58i)$	$P_{11}(1356 - 76i)$	$P_{11}(1364 - 105i)$	$P11$(total)
$A_{1/2}$	$-129 + 44i$	$-31 + 29i$	$-13 + 20i$	$-14 + 22i$	$-28 + 20i$
$A_{3/2}$	$265 + 19i$	$171 + 91i$	–	–	–

TABLE V. The $\gamma N \to \Delta(1232)$ helicity amplitudes (A_λ in 10^{-3} GeV$^{-1/2}$) calculated at Breit-Wigner position $W = 1232$ MeV are compared with previous results.

		EBAC-DCC	Arndt [31]	Ahrens [32]	Dugger [33]	Blanpied [34]
$P_{33}(1232)$	$A_{3/2}$	-251	-243 ± 1	-256 ± 3	-258 ± 5	$-266.9 \pm 1.6 \pm 7.8$
	$A_{1/2}$	-136	-129 ± 1	-137 ± 5	-139 ± 4	$-135.7 \pm 1.3 \pm 3.7$

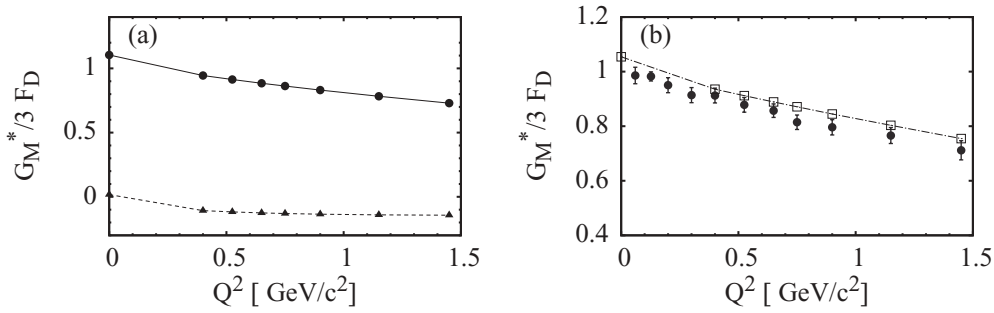

FIG. 9. The magnetic N-$\Delta(1232)$ transition form factor $G_M^*(Q^2)$ defined in Ref. [7]. $F_D = 1/(1 + Q^2/b^2)^2$ with $b^2 = 0.71$ (GeV/c)^2. Left: the solid circles (solid triangles) are the real (imaginary) parts of our results. Right: The data points are from recent analyses [18,38–40] using the Breit-Wigner parametrization. Open squares are our results at $W = 1232$ Mev of the Breit-Wigner position, as discussed in the text.

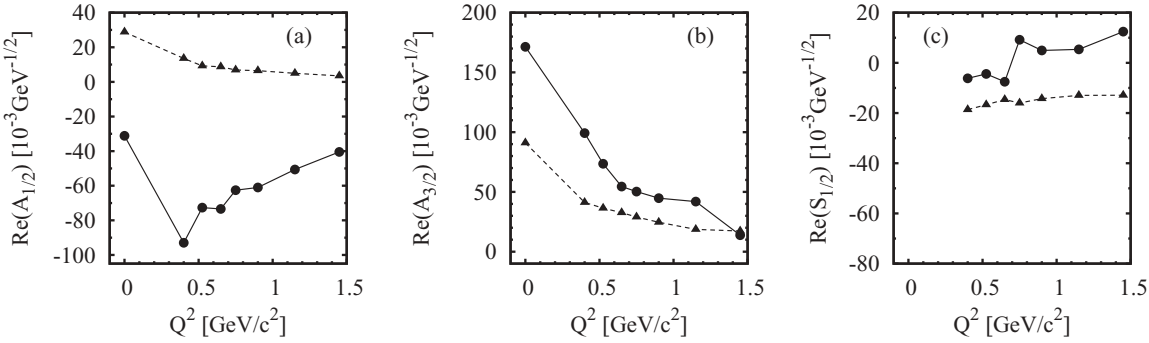

FIG. 10. The extracted $\gamma N \to N^*[D_{13}(1521 - 58i)]$ form factors: (a) $A_{1/2}(Q^2)$, (b) $A_{3/2}(Q^2)$, and (c) $S_{1/2}(Q^2)$. The solid circles (solid triangles) are their real (imaginary) parts.

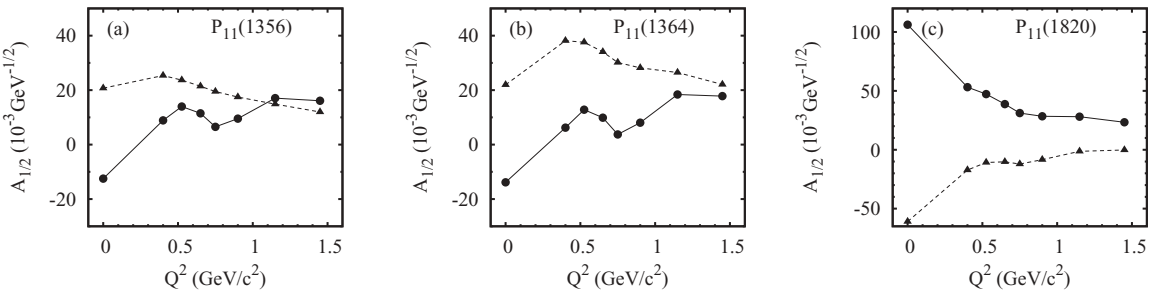

FIG. 11. The extracted $\gamma N \to N^*$ form factors $A_{1/2}(Q^2)$ for three P_{11} resonance poles; (a) $P_{11}(1357 - 76i)$, (b) $P_{11}(1364 - 105i)$, and (c) $P_{11}(1820 - 248i)$. They are on different Riemann sheets as listed in Table I. The solid circles (solid triangles) are their real (imaginary) parts.

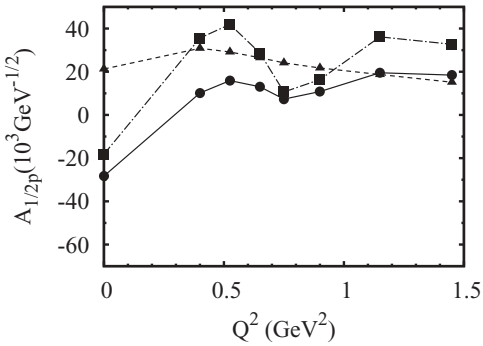

FIG. 12. The form factor $A_{1/2}(Q^2)$ of the P_{11} resonance near the $\pi\Delta$ threshold calculated from using the unified representation Eq. (45) and the residues of two P_{11} poles at $(1357 - 76i)$ MeV and $(1364 - 105i)$ MeV listed in Table I. See text for the procedures for this calculation. Solid circle (solid triangle) shows the real (imaginary) part of the helicity amplitude. Solid square (connected by the dot-dashed line) shows the contribution of the bare form factor.

changing the sign of the real part at $Q^2 \sim 0.4$ (GeV/c)^2. This sign change of the bare $\gamma N \to N^*$ form factor is seen in some relativistic constituent quark model calculations [41,42]. This suggests that our bare parameters can perhaps be interpreted in terms of hadron structure calculations excluding the MB coupled-channel effects, which is determined by the unitarity condition.

To end this section, we emphasize that our $\gamma N \to N^*$ form factors at pole positions presented in Figs. 9 through 12 are well defined in terms of the matrix elements of the current operator between eigenstates of the Hamiltonian, as discussed in Sec. III. This must be accounted for in comparing our results with any hadron structure calculation.

V. SUMMARY

We explained the application of a recently developed analytic continuation method to extract the electromagnetic transition form factors for the nucleon resonances (N^*) within the EBAC-DCC model of the MB reactions. We discuss in detail how the contours for solving the considered coupled-channels integral equations are chosen to find resonance poles M_R and their residues. The formula for determining the $\gamma^* N \to N^*$ transition form factors $A_\lambda(Q^2)$ and $S_\lambda(Q^2)$, defined on the complex Riemann energy sheet, from the extracted residues are presented.

We found that the resulting Laurent expansions of the $\pi N \to \pi N$ and $\gamma N \to \pi N$ amplitudes, evaluated in the physical energy region, can reproduce to a very large extent the exact solutions of the EBAC-DCC model at energies near $E = \mathrm{Re}(M_R)$. A formula was developed to give a unified representation of the effects due to the first two P_{11} resonances, which are near the $\pi\Delta$ threshold, but are on different Riemann sheets. Illustrative results for the well-isolated P_{33} and D_{13}, and the complicated P_{11} resonances are presented.

We discuss the differences between our results and those extracted from the approaches using the Breit-Wigner parametrization of resonant amplitude to fit the data. We find that there is no simple connection between these two different approaches.

To conclude, we emphasize that our form factors are defined in a well-studied theoretical framework [12,13,22] within which a resonance is an "eigenstate" of the Hamiltonian with the outgoing boundary condition for the asymptotic wave function of its decay channels. Thus the electromagnetic transition form factors defined by $\langle \psi^R_{N^*} | J_{\mathrm{em}} | N \rangle$, which can be extracted from the residues of the resonance poles, must be complex since the resonant wave function $\psi^R_{N^*}$ contains a scattering continuum. This must be accounted for in comparing our results with those from using the Breit-Wigner form to fit the data and any hadron structure calculations of the N-N^* transition form factors, such as those from relativistic quark models [41,42], Dyson-Schwinger models [43], and lattice QCD (LQCD) [44].

ACKNOWLEDGMENTS

This work is supported by the US Department of Energy, Office of Nuclear Physics Division, under Contract No. DE-AC02-06CH11357 and Contract No. DE-AC05-06OR23177 under which the Jefferson Science Associates operate Jefferson Lab, and by the Japan Society for the Promotion of Science, Grant-in-Aid for Scientific Research(C) 20540270.

[1] N. Suzuki, T. Sato, and T.-S. H. Lee, Phys. Rev. C **79**, 025205 (2009).
[2] N. Suzuki, B. Julia-Diaz, H. Kamano, T.-S. H. Lee, A. Matsuyama, and T. Sato, Phys. Rev. Lett. **104**, 042302 (2010).
[3] B. Julia-Diaz, T.-S. H. Lee, A. Matsuyama, and T. Sato, Phys. Rev. C **76**, 065201 (2007).
[4] A. Matsuyama, T. Sato, and T.-S. H. Lee, Phys. Rep. **439**, 193 (2007).
[5] B. C. Pearce and I. R. Afnan, Phys. Rev. C **34**, 991 (1986); **40**, 220 (1989).
[6] F. Gross and Y. Surya, Phys. Rev. C **47**, 703 (1993).
[7] T. Sato and T.-S. H. Lee, Phys. Rev. C **54**, 2660 (1996); **63**, 055201 (2001).
[8] C. T. Hung, S. N. Yang, and T.-S. H. Lee, Phys. Rev. C **64**, 034309 (2001).
[9] A. M. Gasparyan, J. Haidenbauer, C. Hanhart, and J. Speth, Phys. Rev. C **68**, 045207 (2003); M. Döring, C. Hanhart, F. Huang, S. Krewald, and U.-G. Meißner, Nucl. Phys. A **829**, 170 (2009).
[10] B. Julia-Diaz, T.-S. H. Lee, A. Matsuyama, T. Sato, and L. C. Smith, Phys. Rev. C **77**, 045205 (2008).
[11] B. Julia-Diaz, H. Kamano, T.-S. H. Lee, A. Matsuyama, T. Sato, and N. Suzuki, Phys. Rev. C **80**, 025207 (2009).
[12] A. Bohm, *Quantum Mechanics: Foundations and Applications* (Springer-Verlag, New York, 1993).

[13] R. H. Dalitz and R. G. Moorhouse, Proc. R. Soc. London A **318**, 279 (1970).
[14] M. Döring, C. Hanhardt, F. Huang, S. Krewald, and U.-G. Meißner, Phys. Lett. B **681**, 26 (2009).
[15] A. V. Anisovich, E. Klempt, V. A. Nikonov, M. A. Matveev, A. V. Sarantsev, and U. Thoma, Eur. Phys. J. A **44**, 203 (2010).
[16] R. A. Arndt, W. J. Briscoe, I. I. Strakovsky, and R. L. Workman, Phys. Rev. C **74**, 45205 (2006).
[17] D. Drechsel, S. S. Kamalov, and L. Tiator, Eur. Phys. J. A **34**, 69 (2007).
[18] I. G. Aznauryan *et al.* (CLAS Collaboration), Phys. Rev. C **80**, 055203 (2009); V. I. Mokeev, V. D. Burkert, L. Elouadrhiri, G. V. Fedotov, E. N. Golovach, and B. S. Ishkhanov, Chin. Phys. C **33**, 1210 (2009).
[19] R. J. Eden and J. R. Taylor, Phys. Rev. Lett. **11**, 516 (1963).
[20] D. Morgan and M. R. Pennington, Phys. Rev. Lett. **59**, 2818 (1987).
[21] J. R. Taylor, *Scattering Theory, The Quantum Theory of Nonrelativistic Collisions* (Wiley, New York, 1972).
[22] K. W. McVoy, in *Fundamentals in Nuclear Theory*, edited by A. De Shalit and C. Villi (IAEA, Vienna, 1967), p. 475.
[23] C. Amsler *et al.*, Phys. Lett. B **667**, 1 (2008).
[24] L. A. Copley, G. Karl, and E. Obryk, Nucl. Phys. B **13**, 303 (1969).
[25] R. A. Arndt, J. M. Ford, and L. D. Roper, Phys. Rev. D **32**, 1085 (1985).
[26] R. E. Cutkosky and S. Wang, Phys. Rev. D **42**, 235 (1990); R. E. Cutkosky, C. P. Forsyth, R. E. Hendrick, and R. L. Kelly, *ibid.* **20**, 2839 (1979).
[27] M. Kato, Ann. Phys. (NY) **31**, 130 (1965).
[28] Y. Fujii and M. Kato, Phys. Rev. **188**, 2319 (1969).
[29] Y. Fujii and M. Fukugita, Nucl. Phys. B **85**, 179 (1975).
[30] D. Bugg, J. Phys. G: Nucl. Part. Phys. **37**, 055002 (2010).
[31] R. A. Arndt, W. J. Briscoe, I. I. Strakovsky, and R. L. Workman, Phys. Rev. C **66**, 055213 (2002); R. A. Arndt, I. I. Strakovsky, and R. L. Workman, *ibid.* **53**, 430 (1996).
[32] J. Ahrens *et al.*, Eur. Phys. J. A **21**, 323 (2004); Phys. Rev. Lett. **88**, 232002 (2002).
[33] M. Dugger *et al.*, Phys. Rev. C **76**, 025211 (2007).
[34] G. Blanpied *et al.*, Phys. Rev. C **64**, 025203 (2001).
[35] K. Joo *et al.* (CLAS Collaboration), Phys. Rev. Lett. **88**, 122001 (2002).
[36] K. Joo *et al.* (CLAS Collaboration), Phys. Rev. C **68**, 032201 (2003).
[37] H. Egiyan *et al.* (CLAS Collaboration), Phys. Rev. C **73**, 025204 (2006).
[38] N. F. Sparveris *et al.*, Phys. Rev. Lett. **94**, 022003 (2005).
[39] S. Stave *et al.*, Eur. Phys. J. A **30**, 471 (2006).
[40] N. F. Sparveris *et al.*, Phys. Lett. B **651**, 102 (2007).
[41] S. Capstick and B. D. Keister, Phys. Rev. D **51**, 3598 (1995).
[42] I. G. Aznauryan, Phys. Rev. C **76**, 025212 (2007).
[43] See the review by P. Maris and C. D. Roberts, Int. J. Mod. Phys. E **12**, 297 (2003).
[44] H.-W. Lin *et al.*, Phys. Rev. D **79**, 034502 (2009).